AIAA 2000–0140

Shock Unsteadiness in a Reattaching Shear Layer

J. Poggie
US Air Force Research Laboratory, Wright-Patterson AFB, OH 45433-7521
A. J. Smits
Princeton University, Princeton, NJ 08544-5263

38th AIAA Aerospace Sciences Meeting and Exhibit
10-13 January 2000 / Reno, NV

Shock Unsteadiness in a Reattaching Shear Layer

J. Poggie*
US Air Force Research Laboratory, Wright-Patterson AFB, OH 45433-7521

A. J. Smits†
Princeton University, Princeton, NJ 08544-5263

The origin of shock unsteadiness in a Mach 2.9 turbulent, reattaching shear layer was investigated experimentally using temporally-resolved flow visualization and measurements of wall pressure fluctuations. In order to isolate the influence of disturbances originating in the incoming shear layer, experiments were conducted in which artificial disturbances were introduced into the flow through air injection in the vicinity of separation. The effect on the reattachment shock system was dramatic: the intensity of the pressure fluctuations and shock motion increased substantially and power spectra of the pressure fluctuations showed a distinct shift to lower frequency. The spectra collapsed onto a common curve in nondimensional coordinates based on a length scale derived from two-point cross-correlations of the flow visualization data and a convection velocity derived from cross-correlations of the pressure measurements. This curve showed fairly good agreement with a theory developed by Plotkin (AIAA J., Vol. 13, No. 8, 1975, pp. 1036-1040), which is based on perturbation of a shock by random fluctuations in the incoming turbulent flow. These results indicate that, unlike separated compression ramp flows where shock motion is associated primarily with relatively low-frequency expansion and contraction of the separation bubble, the shock motion in the reattaching shear layer is primarily caused by organized structures in the incoming turbulent flow.

Nomenclature

f	= frequency
G	= power spectrum
I	= scattering intensity
p	= pressure
R	= correlation
t,τ,ξ	= time
u	= fluctuating velocity component
U	= mean velocity component
x,X	= coordinate along ramp
y,Y	= coordinate perpendicular to ramp
δ	= boundary layer or shear layer thickness
ρ	= density
σ_p	= $(\overline{p'^2})^{1/2}$

Subscripts

c	correlation
e	edge
h	hole
I	intensity
p	pressure
R	shock recovery
r	reattachment
ref	reference
s	separation
u	velocity
x	position

Superscripts

$*$	= nondimensional variable
$\cdot$	= time derivative

Introduction

THE mechanisms of shock unsteadiness in separated boundary layer flow have been a topic of extensive research, motivated primarily by the need to mitigate aircraft fatigue loading caused by the intense fluctuations in wall pressure and heat flux that accompany shock oscillation. The first study of this problem was carried out by Kistler,[1] who measured wall pressure fluctuations in a supersonic forward-facing step flow. Kistler observed an intermittent wall pressure signal in which fluctuations due to turbulence in the incoming boundary layer and separation bubble were modulated by rapid pressure jumps associated with the motion of the separation shock back and forth across the transducer. This pattern has since been observed experimentally in a wide variety of separated supersonic flows over two- and three-dimensional test configurations.[2]

*Research Aerospace Engineer, Air Vehicles Directorate, AFRL/VAAC, 2210 Eighth Street. Senior Member AIAA.

†Professor, Department of Mechanical and Aerospace Engineering, P.O. Box CN5263. Associate Fellow AIAA.

The shock motion occurs on two scales: one because of perturbation of the shock by organized structures in the flow turbulence and the other because of relatively large-scale, low-frequency expansion and contraction of the separation bubble.[3] The large-scale phenomenon appears to be analogous to the cyclic vortex shedding caused by instability of the separation vortex system in low-speed separated flows,[4–7] but may also be connected to turbulence in the separation bubble and in the incoming flow.[8–10]

The small-scale shock motion has been observed directly[11–14] using a planar visualization technique based on Rayleigh scattering. Images obtained with this technique show that the shock is distorted, and often split, by organized turbulence structures as they convect into the separation zone. Difficulty in seeding the separation zone with scattering particles has precluded visualization of the large-scale shock motion with laser scattering techniques. Kussoy et al.,[15] however, have observed the expansion and contraction of the separation bubble using cinematic shadow photography in a configuration where the line of sight averaging inherent in this technique was minimized.

Profiles of the intensity of pressure fluctuations[16] and heat transfer fluctuations[17,18] along a streamwise line at the wall of a separated boundary layer in compressible flow typically show two distinct maxima: one just upstream of the mean separation line and one near the mean reattachment line. These peaks may be an order of magnitude above the fluctuation levels in the incoming turbulent boundary layer flow. Conditional averaging has shown that, in many flows, the peaks are caused by motion of the two legs of a lambda shock system (the separation and reattachment shocks) as the separation bubble expands and contracts.[10,19]

Most research has focused on the motion of the separation shock, with relatively little emphasis on reattachment shock unsteadiness. To address this lack of data, Shen *et al.*[20] investigated the wall pressure fluctuations in a flow where the separation point was essentially fixed at a backward-facing step, but the reattachment point was free to move along a ramp. The character of the shock unsteadiness in the reattaching flow was found to be substantially different from that of a typical separating flow.

The present study was undertaken to extend the work of Shen *et al.*, and to search for mechanisms which might be responsible for shock unsteadiness in the reattaching shear layer. The fluctuations in wall pressure caused by the motion of the reattachment shock system were measured, and the flow was visualized using a laser scattering technique. In order to isolate the influence on the reattachment shock system of disturbances originating in the incoming shear layer, experiments were conducted in which artificial disturbances were introduced into the flow through air injection in the vicinity of separation. This controlled perturbation of the flow makes clear the connection between shock unsteadiness and incoming disturbances in the shear layer, and raises the possibility of future methods of controlling shock unsteadiness.

Theoretical Model

Since the separation location is fixed at the backward-facing step in the reattaching shear layer configuration, the primary mechanism for shock oscillation is believed to be perturbation by disturbances in the incoming turbulent flow. A theoretical model for this process has been developed by Plotkin.[21]

Plotkin assumed that a stable location exists for the shock, the position where the shock would sit if no disturbances were present in the incoming flow. As a large-scale eddy convects into the vicinity of the shock, it changes the jump conditions across the shock, and causes it to move away from the equilibrium position. After the eddy passes, the shock obtains a velocity in its new environment that tends to return it toward the equilibrium position.

For simplicity, Plotkin considered only a one-dimensional model for oscillation in the direction parallel to the wall (x). The shock velocity ($\dot{x}$) was taken to be the superposition of a random forcing function (u) and a restoring velocity that is proportional to the displacement (x) of the shock from its equilibrium position:

$$\dot{x} = u(t) - x/\tau_R \tag{1}$$

Here τ_R is a time constant specifying how rapidly the shock recovers from a perturbation. The variables x and u are defined to have zero mean.

Plotkin considered the random function u to represent convection of the shock by velocity fluctuations in the boundary layer. This function is probably better viewed as the shock velocity induced by changes in the jump conditions due to turbulent fluctuations. For linearized jump conditions, u would be proportional to the velocity fluctuations in the boundary layer. The restoring term in Eq. (1) represents the shock velocity induced by changes in the jump conditions due to changes in the local mean flow associated with displacement of the shock from its equilibrium location.

For a given history of velocity perturbations, Eq. (1) can be solved to give the resulting time-history of shock position. Assuming that $x(0) = 0$, the solution can be put in the form:

$$x = e^{-t/\tau_R} \int_0^t u(\xi) e^{\xi/\tau_R} d\xi \tag{2}$$

Plotkin used Eq. (2) to relate the statistical properties of the shock motion to those of the fluctuations in the turbulent boundary layer, noting an analogy to linearly-damped Brownian motion.

An important parameter characterizing both the velocity fluctuations and the consequent shock motion is

the integral time scale of the autocorrelation function. The integral time scale is defined as:

$$\tau_i = \int_0^\infty R_i(\tau) d\tau \tag{3}$$

where i is replaced by u, x, or p to indicate the autocorrelation of the fluctuations in the turbulent boundary layer, the shock position, or the wall pressure fluctuations. The autocorrelation function is defined in the usual manner for time-series data.

Assuming that the shock response is much slower than the turbulent fluctuations ($\tau \gg \tau_u$ and $\tau_R \gg \tau_u$), Plotkin found an approximate expression for the mean square shock excursion:

$$\overline{x^2} = \overline{u^2}\,\tau_u \tau_R \tag{4}$$

From the same assumptions, he also derived the following simplified form for the autocorrelation of the shock position:

$$R_x(t) = e^{-t/\tau_R} \tag{5}$$

At this level of approximation, the autocorrelation of the shock position is independent of the detailed statistical properties of the boundary layer turbulence, and the integral time scale of the shock position is the same as the time constant of the restoring velocity: $\tau_x = \tau_R$.

Plotkin went on to assume that the pressure distribution induced by the oscillating shock can be approximated by the mean pressure distribution translated to the instantaneous shock position. Expanding the mean pressure distribution in a Taylor series about the mean shock location, and retaining terms through first order, he showed that the mean square fluctuating pressure is proportional to the mean square shock excursion.

$$\overline{p'^2} = \left(\frac{\partial \overline{p}}{\partial x}\right)^2 \overline{x^2} = \left(\frac{\partial \overline{p}}{\partial x}\right)^2 \overline{u^2}\,\tau_u \tau_R \tag{6}$$

(Recently, a related approximation has been used successfully to predict fluctuating loads due to separation shock oscillation.[22]) Further, the autocorrelation of the pressure fluctuations is the same as that of the shock position: $R_p(t) = R_x(t)$ and $\tau_p = \tau_R$. He then calculated the spectrum of the pressure fluctuations from the Fourier transform of the auto-correlation:

$$G(f) = \frac{4\overline{p'^2}\tau_p}{1 + (2\pi f \tau_p)^2} \tag{7}$$

where $2\pi f \tau_p < 1$. Plotkin also assumed that the integral time scales were proportional to a characteristic boundary layer time scale δ/U_e. These results suggest plotting the power spectra of pressure fluctuation measurements in the form $G^* = U_{\rm ref} G/(\overline{p'^2}\delta_{\rm ref})$ versus $f^* = f\delta_{\rm ref}/U_{\rm ref}$ and comparing the data to the equation:

$$G^*(f^*) = \frac{4\tau_p^*}{1 + (2\pi f^* \tau_p^*)^2} \tag{8}$$

where $\tau_p^* = U_{\rm ref}\tau_p/\delta_{\rm ref}$.

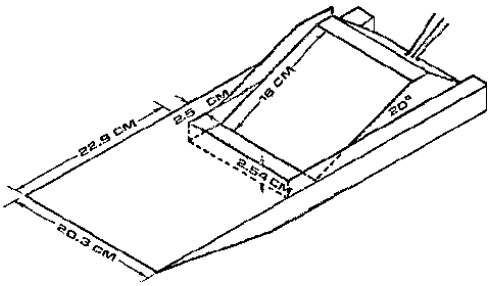

Fig. 1 Diagram of the experimental model. Adapted from Baca.[24]

Alternative treatments of the interaction of organized structures with a shock have used linearized versions of the Euler equations and shock jump conditions to predict the distortion of the shock shape and the amplitude of downstream disturbances caused by a small oncoming perturbation. (See, for example, Erlebacher and Hussaini[23] and the references therein.) Plotkin's work is better viewed as a conceptual model of the shock unsteadiness than as a linearized shock evolution equation. Where a linearized theory would predict the spectrum of shock unsteadiness to be the same as that of the incoming turbulence, Plotkin's model is able to relate the spectrum of shock motion to the mean flow conditions through the parameter τ_p. In this way, the model incorporates some of the nonlinear aspects of the interaction of organized structures and a shock.

Experimental Methods

The experiments were carried out in the Princeton University Gas Dynamics Laboratory Mach 3 blowdown wind tunnel. High-pressure air is supplied to the

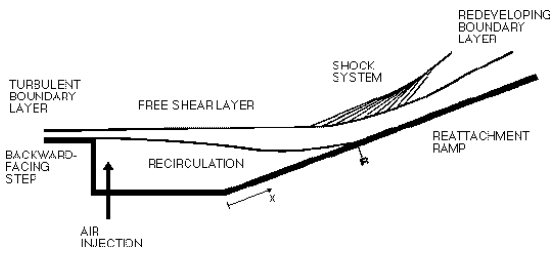

Fig. 2 Sketch of a cross-section of the mean flowfield. Mean reattachment location marked as 'R'. Adapted from Baca.[24]

facility by as many as five Worthington 75 kW four-stage compressors. The compressed air passes through a chemical drying system, and is stored at pressures of up to 20 MPa in four tanks with a total capacity of 57 m^3. A hydraulically-controlled valve regulates the tunnel stagnation pressure as the air flows from the storage tanks into the settling chamber. The experiments were carried out in the first of the wind tunnel's three 902 mm long test sections, which has a square cross-section of 203 mm by 203 mm. The pressure in the settling chamber was maintained at 0.69 ± 0.03 MPa for all experiments, and the freestream Mach number was 2.92 ± 0.01. In a two-minute typical run, the stagnation temperature was initially 290 K and dropped by about 8%.

The experimental configuration for the reattaching shear layer is illustrated in Figs. 1 and 2. The experimental model was originally designed by Baca.[24] In this flow, a Mach 2.9 turbulent boundary layer forms on a flat plate and detaches at a backward-facing step. As a result, a free shear layer forms over a region of recirculating flow. The shear layer reattaches on a 20° ramp, passing through an oblique shock system, and a turbulent boundary layer develops on the ramp downstream. Surveys of the basic properties of the flowfield were performed in earlier experimental programs at the Princeton Mach 3 wind tunnel[20,24–27] and similar configurations have been investigated in other facilities.[28–30]

Measurements have indicated that a zero-pressure-gradient, equilibrium turbulent boundary layer is present in the vicinity of the backward-facing step with a thickness of about $\delta_s = 3$ mm (based on the location of 98% of the freestream Pitot pressure) and a momentum thickness Reynolds number of about 10^4. Due to the position of the reattachment ramp, the boundary layer separates at the 25 mm step with a minimal change in flow direction. The mean velocity profiles of the resulting free shear layer become self-similar about $18\delta_s$ (58 mm) downstream of the step, where the nominal convective Mach number[31] is about 1.1 and the growth rate is in good agreement with data from other compressible, turbulent mixing layer experiments.[25] According to surface flow visualization data, the mean reattachment line lies 67 ± 1 mm up the 20° ramp. The boundary layer on the ramp is strongly perturbed near reattachment, but approaches the equilibrium condition farther downstream.

In order to provide optical access to the flow, the experimental model was modified by Shen *et al.*[20] from the original design of Baca. The cavity of the model was fitted with removable inserts so that the height of the sidewall could be set at either 15.9 mm or 25.4 mm (see Figure 1). The experiments reported here were carried out with the sidewall inserts and the aerodynamic fences on the sides of the ramp removed. Experimental checks[32] showed that the alterations did not significantly change the flowfield, although a slight deflection angle was introduced where the flow detached from the backward-facing step, changing the static pressure ratio across the step from 1.01 to 1.04.

Flow Visualization

A series of experiments was carried out in which the reattachment shock system was visualized using Rayleigh scattering from nanometer-scale contaminant particles in the flow. Illumination was provided by an ultraviolet laser beam focused into a thin sheet in the wind tunnel. The experimental arrangement used optics with a UV-coating, and quartz windows provided optical access to the tunnel test section. Two lasers were used in the course of the experimental program: a Lambda-Physik argon fluoride laser with a wavelength of 193 nm and a frequency-quadrupled Continuum Nd:YAG laser with a wavelength of 266 nm. Both lasers provided a pulse on the order of several nanoseconds in duration at a repetition rate of 10 Hz, and delivered 20-50 mJ of energy per pulse. A double-intensified ITT CID (Charge Integrated Device) camera recorded the light scattered from the laser sheet. The camera had a resolution of 388 by 244 pixels, and the light intensifier had a resolution of 180 lines. The video data were recorded on VHS video tape, and later digitized for analysis.

Additional experiments were carried out in which

the Continuum Nd:YAG laser was used in double-pulse mode, producing pairs of pulses separated by an interval of 12 μs to 60 μs.[13,33] For this case, two cameras, gated to record the two pulses in sequence, were mounted on opposite sides of the wind tunnel and aligned to record the same field of view. In order to ensure that the cameras were properly aligned, an image of a precision grid in the test section was recorded before and after each wind tunnel run. The accuracy of positioning was found to be within 1% of the width of the field of view in all the tests.

The scattering signal is believed to be dominated by Rayleigh scattering from a uniform fog of clusters of H_2O, CO_2, or O_2 molecules that form in the freestream flow as the air cools in the expansion through the wind tunnel nozzle.[34,35] Observations from past work have indicated that the scattering intensity (and thus the particle number density) tends to follow the air density, except where the temperature reaches a level high enough to vaporize the contaminant particles.[12,36] Since the molecular constituents of air have a much smaller scattering cross-section than the relatively larger particles, images of high temperature regions of a flow may appear dark.

For freestream temperatures on the order of 100 K, the fluid near the edge of a Mach 2.9 turbulent boundary layer or free shear layer has a temperature high enough to vaporize the molecular clusters, and a sharp vaporization interface reveals organized structures in the two turbulent shear flows. For relatively weak shocks, the Rayleigh scattering images show an increase in scattering intensity due to the shock density jump, but for stronger shocks, the images show a marked decrease in scattering intensity across the shock, due to vaporization of the scattering particles.

A body of evidence has been accumulated that indicates that the scattering images have accurately portrayed many of the physical features of a turbulent boundary layer, a turbulent mixing layer, and several shock-wave / boundary-layer interactions studied in the Princeton supersonic wind tunnel.[37] In particular, quantitative measures of the scale, orientation, and speed of large-scale organized structures derived from a statistical analysis of scattering images of the turbulent boundary layer and turbulent mixing layer agree well with results obtained in the same flows using hotwire anemometry. Further, Nau[36] has examined simultaneous hotwire and Rayleigh scattering measurements of the turbulent boundary layer, and found a strong correlation between traces of the hotwire signal and the corresponding scattering profiles.

Measurements of Wall Pressure Fluctuations

Static pressure measurements were made with miniature differential pressure transducers manufactured by Kulite Semiconductor Products (model XCQ-72-062-25D). The transducers were calibrated statically at the operating temperature. Previous studies, and checks made before and after wind tunnel runs, have shown that the calibration is consistently linear and repeatable.

The transducers were mounted in a block that could be positioned at different streamwise positions along the reattachment ramp. The spacing between the transducers was 5.1 mm, and they were mounted 2.5 mm off the centerline of the wind tunnel. The data were taken with the block positioned in three locations. Three of the four available transducers were found to calibrate accurately, and were used to cover a range of positions between 52 mm and 88 mm from the start of the ramp.

The signals from the transducers were amplified, then band-pass filtered with a four-pole Butterworth filter. The analog data were then sampled digitally with 10 bit resolution using a CAMAC (Computer Automated Measurement and Control) system from LeCroy, Inc. Three sampling rates were used: 10 kHz, 250 kHz, and 1 MHz. In all three cases the high-pass filter was set to 10 Hz, while the low-pass filter was set to 5 kHz for the 10 kHz sampling rate, and to 80 kHz otherwise. Data were obtained simultaneously for the three channels in files of four records, each containing 24576 contiguous points per record.

Artificial Disturbances

Artificial disturbances were introduced into the flow through air injection in order to isolate the effect of upstream disturbances on the unsteadiness of the shock system. Two spanwise rows of holes for air injection were added to the experimental model. One row was located 12.7 mm upstream of the backward-facing step, and the other was located 12.7 mm downstream of the step. Each row was 101.6 mm long, and consisted of 33 holes, 1.6 mm in diameter. Although tests were made using a number of air injection patterns,[32] for the experiments described here, air was injected from the holes downstream of the backward-facing step in two configurations: one and three holes on the centerline of the model.

Air was supplied to the holes from the wind tunnel storage tanks, by way of a stagnation tank. A series of three pressure regulators in the supply lines brought a typical storage pressure of about 20 MPa down to the desired tank pressure of about 0.7 MPa. The blowing stagnation tank consisted of a 1.02 m length of 8 in (203 mm) nominal diameter pipe with the ends sealed with flanges and blinds.

Air was allowed to leave the tank through sections of 1.6 mm diameter stainless steel tubing. Plastic tubing of 1.6 mm inside diameter connected the stainless steel tubing to similar tubing soldered into the holes in the experimental model.

The supply pressure was maintained at 0.69 ± 0.03 MPa for the tests reported in this paper. Re-

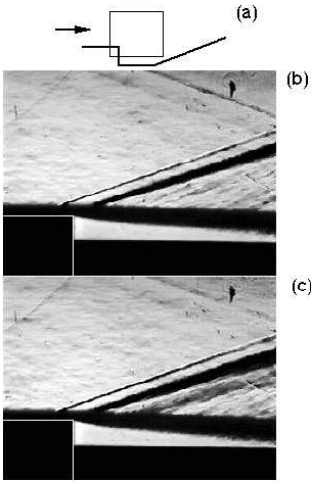

Fig. 3 Schlieren photographs of the flow in the vicinity of the step. (a) Sketch of field of view, not to scale. (b) Undisturbed flow. (c) Air injection through three holes.

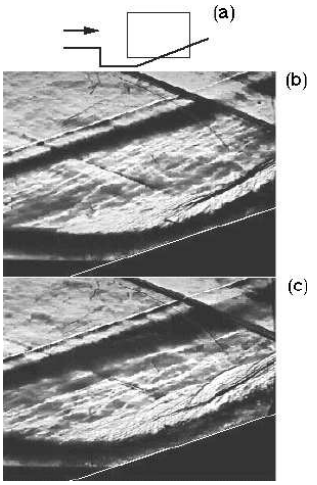

Fig. 4 Schlieren photographs of the flow in the vicinity of the ramp. (a) Sketch of field of view, not to scale. (b) Undisturbed flow. (c) Air injection through three holes.

sults of calibration[32] indicate that the ratio of the mass flux through a hole to the mass flux in the freestream was on the order of $\rho_h U_h/(\rho_e U_e) = 0.07$, and the momentum flux ratio was on the order of $\rho_h U_h^2/(\rho_e U_e^2) = 0.04$.

Results

Schlieren Photography

Schlieren photographs were taken in order to provide an overview of the flowfield and to demonstrate the general effects of air injection. Images were obtained for the region of the flow in the vicinity of the backward-facing step and for the region near the reattachment ramp. Example images are shown in Figs. 3 and 4. In each case a sketch of the field of view is shown at the top of the figure, the upper image was obtained in the undisturbed flow, and the bottom image was obtained for the case with air injection through three holes. The field of view for both the images of the region near the step and the region near the ramp is approximately 100 mm wide by 80 mm high ($10.6\delta_r$ by $7.7\delta_r$, where the boundary layer thickness in the vicinity of the mean reattachment line in the undisturbed flow is $\delta_r = 10.4$ mm).

Figure 3b shows a view of the undisturbed flow in the vicinity of the backward-facing step. The uneven outer edge of the incoming turbulent boundary layer can be seen on the flat plate at the left in the field of view. A Mach wave originates at the row of holes upstream of the step. The boundary layer separates at the step with a slight change in flow direction, and an expansion fan appears centered on the edge of the backward-facing step.

The upper and lower edges of the developing free shear layer are clearly visible in the image. Since a schlieren image represents a spanwise average of the density gradients in the flow, there is relatively little indication of the large-scale structure of the turbulent flow. There are, however, waves visible emanating from the upper edge of the shear layer that are probably associated with organized structures.

Figure 3c shows the effect of air injection on the flow in the vicinity of the step. The jets of injected air are not visible in the image because of the orientation of the schlieren knife edge. A three-dimensional shock system forms due to the jets, and is discernible as a dark curve roughly parallel to the expansion fan upstream. One surprising observation is that the shear layer shifts down (note the increased size of the expansion fan), even though mass is being added to the recirculating region, suggesting that there is enhanced entrainment of freestream fluid into the shear layer. The shear layer also appears to thicken.

The reattachment zone for the undisturbed flow case

is shown in Fig. 4b. The expansion fan centered on the backward-facing step is apparent in the freestream flow, as are two Mach waves originating from joints in the ceiling of the test section. The free shear layer can be seen entering from the left side of the image; most of the shear layer is visible above the cavity sidewall. The highly turbulent nature of the shear layer in the vicinity of reattachment is plain, despite the spanwise averaging process inherent in the schlieren technique.

The reattachment shock system is evident in the image as the light, fan-like region above the redeveloping boundary layer. The shock system appears to be distributed in this manner for two reasons: the primary oblique shock is wrinkled along the spanwise direction, and the system is composed of a combination of a number of shocks and compression waves (see the Rayleigh scattering results below).

The effect of air injection on the reattachment region is quite dramatic (Fig. 4c). The increased thickness of the shear layer and the developing boundary layer is obvious, as is the great distortion of the reattachment shock system. In the example image shown, the primary oblique shock appears to have split into several sections. Severe curvature and strong displacement of the shock system indicate a much higher degree of unsteadiness. The increase in unsteadiness is quite spectacular in the original video recording.

Single-Pulse Laser Scattering

The laser scattering technique used in the present work offers a visualization of an instantaneous planar section of the flow, revealing cross-sections of coherent structures and shock waves. A series of single-pulse laser scattering experiments was carried out to examine the scale and orientation of organized structures in several cross-sectional planes in the reattachment region of the flow, and to look for an association of these structures with shock waves. Two optical configurations were used: one with a vertical laser sheet located along the wind tunnel centerline and the field of view aligned with the reattachment ramp, and another with a horizontal laser sheet located in the outer part of the redeveloping boundary layer.

The side-view images were obtained with a relatively small field of view that allowed the resolution of smaller-scale features of the interaction of the shock system with the incoming turbulent flow. The camera was tilted 20° from horizontal, in alignment with the reattachment ramp. The field of view was approximately 26 mm wide by 20 mm high, and began 54 mm up the reattachment ramp. Sample images are shown in Fig. 5, with the inclined orientation of the field of view sketched at the top of the figure. The mean reattachment location for the undisturbed flow is marked 'R' in the figure, and the ramp surface is indicated with a line.

Figure 5b shows the undisturbed flow. The free

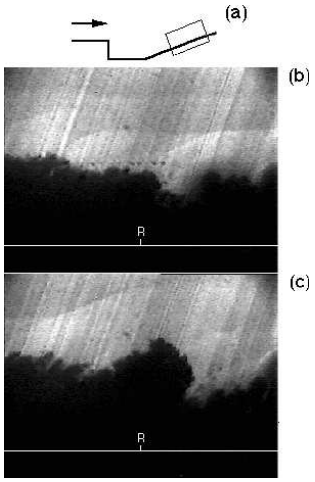

Fig. 5 Side-view laser scattering images of flow along reattachment ramp. (a) Experimental configuration, not to scale. (b) Undisturbed flow. (c) Air injection through three holes.

shear layer can be seen entering from the upper left of each image, and the redeveloping boundary layer exits horizontally from the right. Shocks are seen to form at the interface between slow-moving fluid in the δ-scale bulges of the redeveloping boundary layer and the high-speed fluid of the freestream. These shocks are relatively weak, and are made visible by an increase in the intensity of scattered light due to the increased density of scattering particles downstream of the shocks. Shocks are associated with organized structures having a wide range of length scales, and the strongest shocks are associated with structures with scales on the order of the thickness of the redeveloping boundary layer ($\delta_r = 10.4$ mm).

Figure 5c shows an example image for the case with air injection through one hole in the cavity of the experimental model. There is a dramatic increase in the thickness of the redeveloping boundary layer, the scale of the turbulence structures, and the strength of the shock waves. Again, there is an association of shocks with large-scale structures in the shear layer.

For plan views of the reattaching flow, a horizontal laser sheet generated with the Spectra Physics ArF laser was positioned 38 mm off the floor of the cavity in the experimental model. The field of view was 31 mm from top to bottom, and began 121 mm downstream of the backward-facing step (see Fig. 6a). The flow

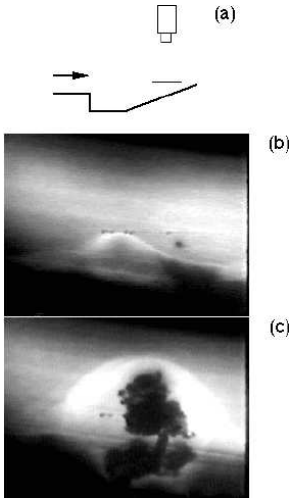

Fig. 6 Horizontal section through reattachment shock system. Field of view aligned with model centerline. (a) Experimental configuration, not to scale. (b) Undisturbed flow. (c) Air injection through one hole.

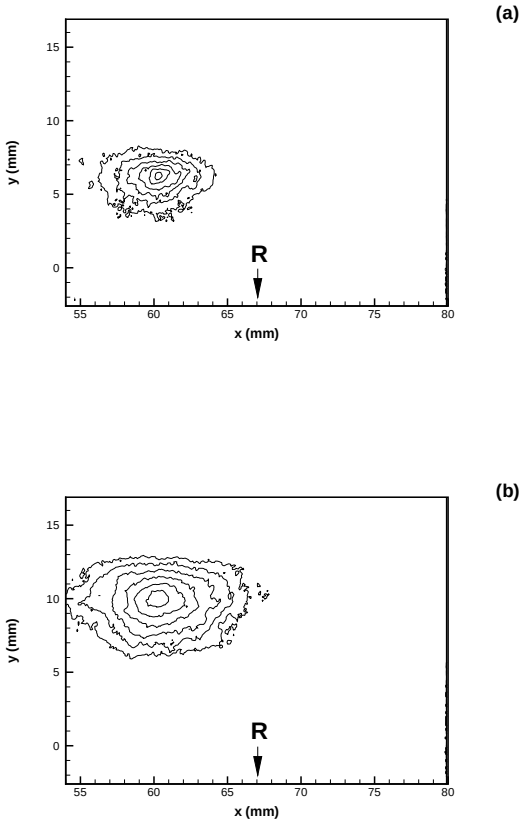

Fig. 7 Two-point auto-correlation of side-view images. (a) Undisturbed flow. (b) Air injection.

direction is from top to bottom in the images, with a component that passes up through the laser sheet from below. For these images the laser sheet is relatively far from the wall, where the compression due to the 20° turning angle occurs over a relatively short streamwise distance. Consequently, the shocks are strong enough here to vaporize the scattering particles, and in the images the flow appears dark downstream of the shocks.

The flow over this portion of the experimental model is highly complex and unsteady, even in the absence of air injection (Fig. 6b). The shock system exhibits spanwise wrinkling with a length scale on the order of the reattachment boundary layer thickness. An image of the flow with air injection through the center hole downstream of the backward-facing step is shown in Fig. 6c. In this image, a bow shock is clearly seen associated with the upstream side of a structure in the redeveloping boundary layer.

In order to quantify the increase in structure length scale seen in the images, two-point cross-correlations were carried out for the set of side-view images of the reattachment region (see Fig. 5). The cross-correlation between the scattering intensity at a reference point $I(X,Y)$ and the scattering intensity at a given point in the field of view $I(x,y)$ was defined as:

$$R_I(x,y,X,Y) = \frac{\mathrm{Cov}[I(x,y),I(X,Y)]}{\sqrt{\mathrm{Var}[I(x,y)]\mathrm{Var}[I(X,Y)]}} \qquad (9)$$

where the covariance and variance are defined in the usual way, e.g.: $\mathrm{Var}(I) = \sum_{i=1}^{N}(I_i - \overline{I})^2/N$. This type of correlation is similar to the zero time-delay cross-correlation between a pair of point probes for different probe separations.

The horizontal position of the reference point was taken to be $X = 60.5$ mm. In order to allow a consistent comparison between the two cases, the vertical coordinate was taken to be the location of maximum root-mean-square scattering intensity (about $Y = 6$ mm for the undisturbed flow and $Y = 10$ mm for the case with air injection).

The results are shown in Fig. 7. Contours are shown from 0.4 to 0.9, with an interval of 0.1. The correlation contours generally have an elliptical shape, as seen in other studies of free shear layers and boundary layers.[11,30] One feature of note, however, is the horizontal orientation of the contours. Typically, the structure orientation is in the neighborhood of 45° from the mean flow direction. The present results reflect the adjustment of the mean flow from a direction parallel to the freestream to a direction aligned with the ramp

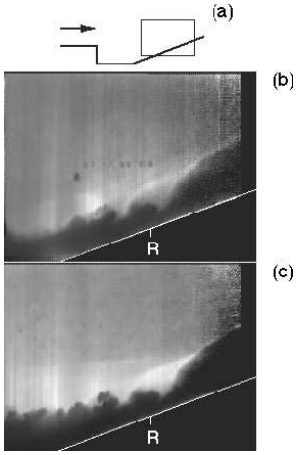

Fig. 8 A pair of images of the undisturbed flow taken with the dual camera configuration and the laser in single-pulse mode. (a) Field of view, not to scale. (b) Camera One. (c) Camera Two.

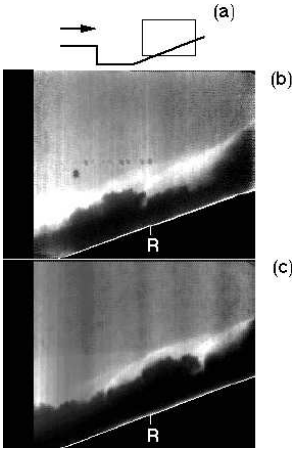

Fig. 9 Pair of double-pulse images obtained in the undisturbed flow using a delay of 30.2 μs. (a) Field of view, not to scale. (b) Camera One. (c) Camera Two.

(see Fig. 5a): the structures are actually inclined to the local mean flow direction.

The primary difference between the baseline case and the perturbed flow is a dramatic increase in the structure length scale. For example, the horizontal length scale of the $R_I = 0.5$ contour increases from about $\delta_c = 6$ mm for the undisturbed flow to about $\delta_c = 9$ mm for the case with air injection.

Double-Pulse Laser Scattering

Double-pulse laser scattering experiments were carried out using a vertical laser sheet to obtain side views of the flow over the ramp. For these experiments, the field of view was aligned with the floor of the cavity in the experimental model rather than with the reattachment ramp. The field of view was 58 mm wide by 43 mm high, and began 92 mm downstream of the backward-facing step. The bottom edge of the field of view lay 14 mm above the cavity floor.

To illustrate that the cameras were aligned and the magnifications matched, Fig. 8 shows a pair of example images of the undisturbed flow for the case with zero time delay (single-pulse mode). Both large-scale turbulence structures and the reattachment shock system are visible in the images, and the fields of view are seen to be closely aligned. The free shear layer enters the field of view from the lower left side of each image, and reattaches on the 20° ramp, forming a new boundary layer which exits near the upper right of the images. The great variability of the thickness of the turbulent boundary layer visible in the reattachment region is consistent with the high degree of intermittency found by Hayakawa *et al.*[27] in hotwire data obtained in this region of the undisturbed flow. As in the images shown above, shocks are seen to form at the upstream sides of the bulges in the redeveloping boundary layer.

Figure 9 shows a pair of images of the undisturbed flow taken with a time delay of 30.2 μs. The top image was captured with one video camera, and the bottom image was captured after the time delay with the other camera. This pair of images was selected because it shows a particularly large structure entering the reattachment zone, where a relatively strong shock forms on its upstream side. Note that a shock associated with the upstream edge of the structure appears to convect along with it as the structure moves downstream.

A similar set of images was obtained in the flow perturbed by air injection through the center hole in the cavity of the experimental model. A pair of images showing a structure entering the reattachment zone is shown in Fig. 10. Although the length scale of the structures is much larger in the disturbed flow, the qualitative behavior of the structures is similar to that

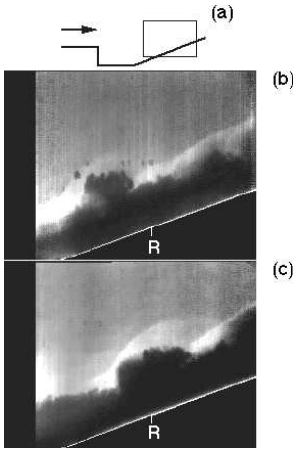

Fig. 10 Pair of double-pulse images obtained in the flow with air injection through one hole using a delay of 30.2 μs. (a) Field of view, not to scale. (b) Camera One. (c) Camera Two.

seen in the undisturbed flow: a shock is present on the upstream edge of a given structure, and moves with the structure as it convects downstream along the ramp.

Pressure Measurements

Measurements were made along the reattachment ramp of the mean and fluctuating surface pressure for the undisturbed flow and for the case with air injection through three holes in the cavity of the experimental model. Figure 11a shows the results for the mean pressure, which are normalized by the static pressure in the freestream flow. The pressure is seen to rise monotonically from the freestream level to the level downstream of the primary oblique shock. With air injection, the pressure rise begins sooner, but the pressure increases more slowly along the streamwise direction, and reaches approximately the same level downstream.

The pressure distributions were found to collapse onto one curve when plotted against the nondimensional distance $(x - x_r)/\delta_c$, where the mean reattachment location was taken to be $x_r = 67$ mm for the undisturbed flow and $x_r = 75$ mm for the case with air injection (Fig. 11b). The following equation was found to provide a good fit to the reduced data:

$$\frac{p}{p_{\rm ref}} = \frac{11}{4} + \frac{7}{4}{\rm erf}\left(\frac{x - x_r}{4\delta_c} + 0.1\right) \qquad (10)$$

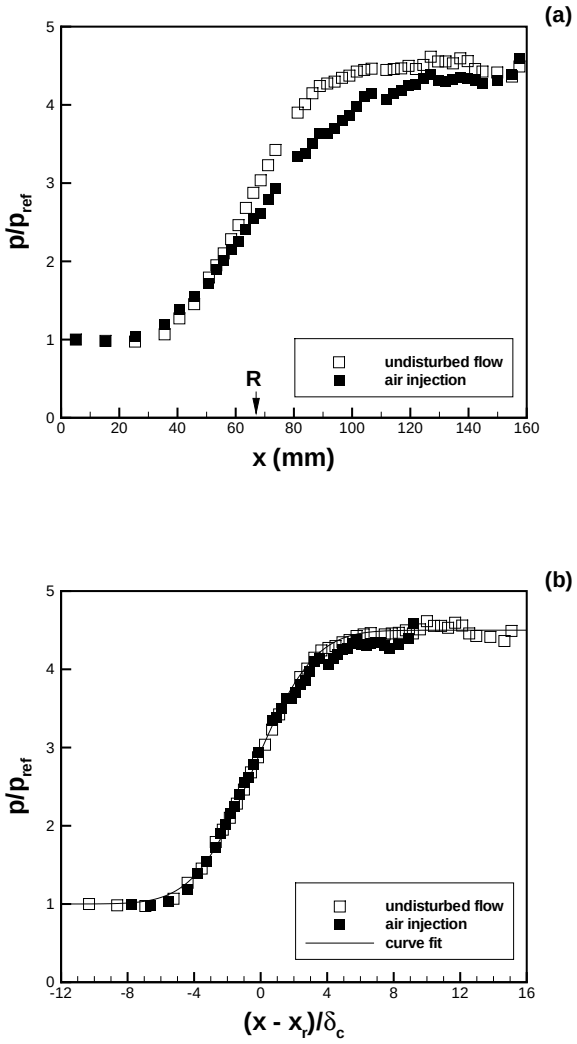

Fig. 11 Mean wall pressure distribution along ramp. (a) Dimensional distance. Mean reattachment location marked as 'R'. (b) Nondimensional distance.

These results indicate that broader pressure distribution observed with air injection reflects primarily the increase in the thickness of the reattaching shear layer, rather than - for example - a large-scale shear layer flapping motion.

Figure 12 shows the standard deviation of the wall pressure fluctuations in the undisturbed flow plotted versus position along the ramp. The measurements of Shen *et al.*[20] are shown for comparison. The data have been normalized by the static pressure in the freestream flow. An error bar of $\pm 0.05 p_{\rm ref}$ indicates the level of scatter in the data. The intensity of the pressure fluctuations in the present flow is somewhat higher than that found by Shen *et al.*, primarily because of the removal of the aerodynamic fences and sidewall inserts to allow optical access to the flow.[32] Nevertheless, both data sets show a rise in the pressure fluctuation levels to a peak downstream of the mean reattachment line, followed by a gradual de-

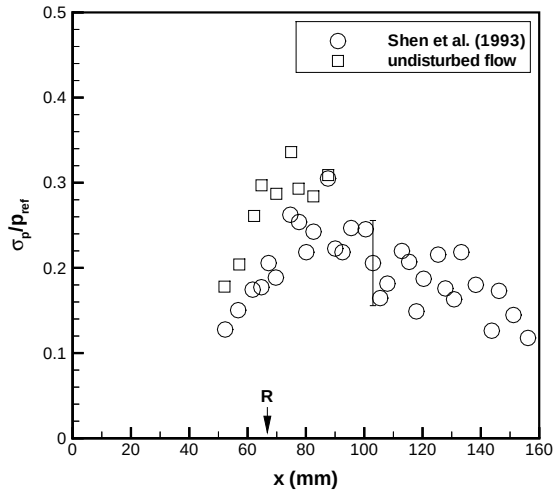

Fig. 12 Intensity of wall pressure fluctuations along ramp. Mean reattachment location marked as 'R'.

crease downstream.

Figure 13a compares the pressure fluctuation levels in the undisturbed flow to the case with air injection into the flow through three holes on the cavity centerline. The distribution of the intensity of the pressure fluctuations has the same shape in the air injection case as in the undisturbed flow case, but is shifted upward significantly. There is an increase of about 50% in the standard deviation of the pressure signal at the station farthest upstream. Given that the pressure fluctuations are caused primarily by shock motion, this change is consistent with the apparent increase in shock unsteadiness observed in the flow visualization data, and indicates a strong connection between the incoming disturbances and the shock motion in the flow.

Plotkin's model gives an estimate of the intensity of the pressure fluctuations, Eq. (6), provided that the streamwise component of the mean pressure gradient and the amplitude of the shock motion are known. Here we take δ_c as a measure of the amplitude of the shock motion, and use the derivative of Eq. (10) to determine the streamwise pressure gradient: $\sigma_p/p_{\rm ref} \approx (\partial\overline{p}/\partial x)\delta_c/p_{\rm ref}$. The results are shown in Fig. 13b, plotted against the nondimensional streamwise position. Since the mean pressure distribution collapsed in nondimensional coordinates, its derivative $\partial\overline{p}/\partial x$ also does, and the theory predicts the single curve shown in the figure. The theory gives the correct order of magnitude for the location and value of the peak pressure fluctuation intensity, but does not predict the increase in intensity observed with air injection.

Cross-correlation calculations were made between adjacent pairs of pressure transducers. Figure 14 shows an example cross-correlation plot for a pair of transducers located 82.6 mm and 87.6 mm up the

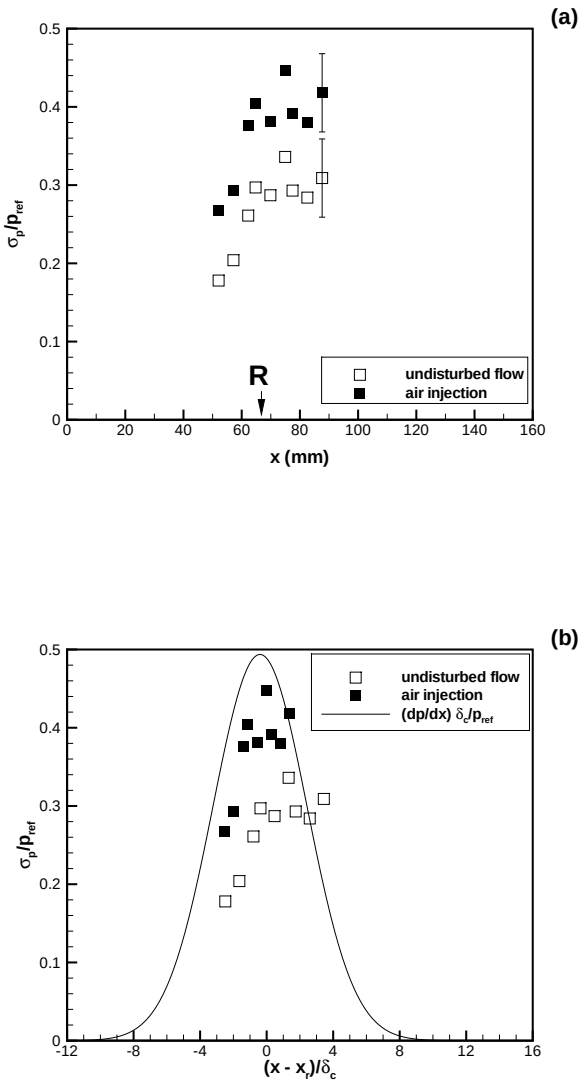

Fig. 13 Effect of air injection on wall pressure fluctuations. (a) Dimensional distance. Mean reattachment location marked as 'R'. (b) Nondimensional distance.

ramp. This location was chosen because it lies near the point of maximum intensity in the wall pressure fluctuations. The single peak in the cross-correlation indicates the downstream convection of the large-scale structures in the redeveloping boundary layer. The effect of air injection was to increase the peak correlation, increase the speed of the structures (reduce the optimum time delay), and to increase the width of the correlation function. With air injection, the convection velocity (adjusted to a nominal stagnation temperature of 270 K) increased from 478 m/s to 577 m/s, and the width of the curve at the $R_p = 0.5$ correlation level increased from 14 μs to 20 μs.

An important parameter identified by Plotkin[21] in setting the characteristic frequency of the power spectrum is the integral time scale of the auto-correlation (see above). Auto-correlations for the transducer lo-

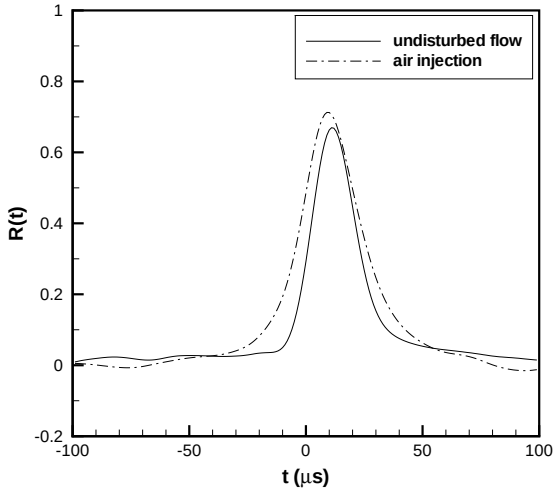

Fig. 14 Cross-correlations of pressure signals at $x = 82.6$ mm with $\Delta x = 5.1$ mm.

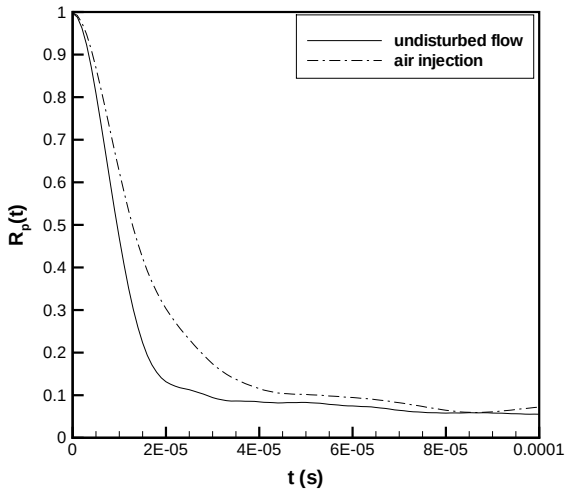

Fig. 15 Auto-correlations of pressure signals at $x = 82.6$ mm.

cated at $x = 82.6$ mm are shown in Fig. 15. A significant increase in the characteristic time scale of the auto-correlation is seen with air injection: the integral time scale increases from about 11 μs to 15 μs. The nondimensional time scale, however, remains approximately constant at $\tau_p^* \approx 0.9$.

Figure 16 shows the corresponding auto-spectra of the fluctuating pressure signal. The data are seen to have a very broad-band energy content, with no prominent peaks. The roll-off at higher frequency is a property of the flow, not the signal processing system: the fourth-order Butterworth filter passes about 70% of the input amplitude at the cutoff frequency of 80 kHz. Air injection is seen to shift the spectrum up, reflecting the increase in the intensity of pressure fluctuations, and to the left, reflecting a decrease in

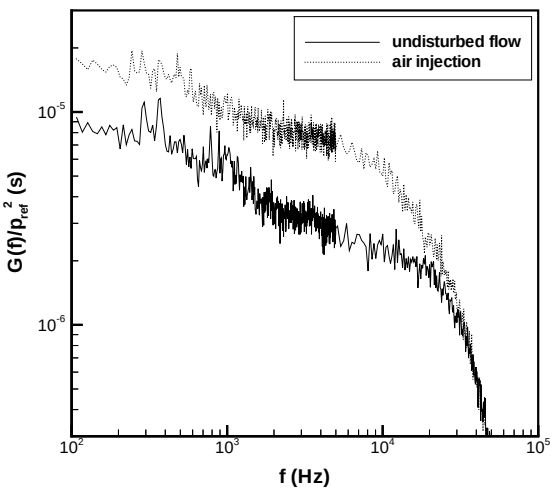

Fig. 16 Auto-spectra for the wall pressure fluctuation data at $x = 82.6$ mm.

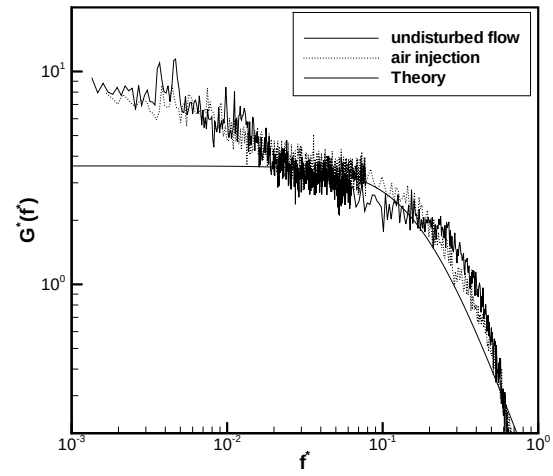

Fig. 17 Normalized auto-spectra for the wall pressure fluctuation data at $x = 82.6$ mm.

characteristic frequency.

Figure 17 shows the spectral data plotted in the normalized form of Eq. (8). The frequency was nondimensionalized by the correlation length scale δ_c and the convection velocity U_c. The spectrum was divided by the mean square fluctuating pressure $\overline{p'^2}$ and the time scale δ_c/U_c. The data collapse well. Nondimensionalizing the frequency causes the 'knees' in the spectrum (present near 2 kHz and 20 kHz in the undisturbed flow) to line up. Plotkin's model is seen to offer a fairly good approximation of the spectrum for $0.02 < f^* < 0.6$ using the measured time scale of $\tau_p^* = 0.9$.

Conclusions

The origin of shock unsteadiness in a Mach 2.9 turbulent, reattaching shear layer was investigated exper-

imentally using temporally-resolved flow visualization and measurements of wall pressure fluctuations. The results indicate that the shock motion in the reattaching shear layer is primarily caused by organized structures in the incoming turbulent flow, in contrast to the related class of separated compression ramp flows, where shock motion is associated primarily with relatively low-frequency expansion and contraction of the separation bubble.

In order to isolate the influence of disturbances originating in the incoming shear layer, experiments were conducted in which artificial disturbances were introduced into the flow through air injection in the vicinity of separation. The effect on the reattachment shock system was dramatic: the intensity of the pressure fluctuations and shock motion increased substantially, and power spectra of the pressure fluctuations showed a distinct shift to lower frequency. Mean pressure profiles on the reattachment ramp collapsed onto a common curve in nondimensional coordinates based on a length scale derived from two-point cross-correlations of the flow visualization data. Similarly, the power spectra of the pressure fluctuations collapsed in coordinates based on this same length scale and a convection velocity derived from cross-correlations of the pressure measurements.

The data were compared to a theory developed by Plotkin,[21] which is based on perturbation of a shock by random fluctuations in the incoming turbulent flow. Spectra of the wall pressure fluctuations predicted by the theory showed fairly good agreement with the experimental data over a relatively broad frequency band. Discrepancies between the model and the data at lower frequency ($f < 1$ kHz) may reflect the wind tunnel background noise field or a shear layer flapping motion. The theory predicted the correct order of magnitude for the location and value of the peak pressure fluctuation intensity, but did not predict the increase in intensity observed with air injection. The reason for this shortcoming may be the use (in the present work) of the length scale δ_c to estimate the amplitude of the shock motion $(\overline{x^2})^{1/2}$.

An important limitation of the theory is the restriction of the shock motion to one dimension. The primary source of pressure fluctuations in the present flow appears to be the highly three-dimensional shocks associated with the upstream sides of δ-scale structures convecting through the reattachment zone.

Acknowledgments

This research was funded in part by grants from the AFOSR and NASA Langley. J. Poggie received support from an NSF Graduate Research Fellowship and the USAF Palace Knight program during the course of this research program.

W. Stokes and R. Bogart provided technical support for this project. The Princeton University laser physics group, and in particular J. Forkey, provided assistance in the laser visualization experiments. The first author would like to thank R. Kimmel and A. Creese for advice in the preparation of this paper.

References

[1]Kistler, A. L., "Fluctuating Wall Pressure Under a Separated Supersonic Flow," *The Journal of the Acoustical Society of America*, Vol. 36, No. 3, 1964, pp. 543–550.

[2]Dolling, D. S., "Unsteady Phenomena in Shock Wave / Boundary Layer Interaction," *Special Course on Shock-Wave / Boundary-Layer Interactions in Supersonic and Hypersonic Flows,* R-792, AGARD, Neuilly Sur Seine, France, 1993, pp. 4–1 – 4–46.

[3]Poggie, J. and Smits, A. J., "Wavelet Analysis of Wall-Pressure Fluctuations in a Supersonic Blunt-Fin Flow," *AIAA Journal*, Vol. 35, No. 10, 1997, pp. 1597–1603.

[4]Eaton, J. K. and Johnston, J. P., "Low Frequency Unsteadiness of a Reattaching Turbulent Shear Layer," *Turbulent Shear Flows 3*, Springer, Berlin, 1982, pp. 162–170.

[5]Driver, D. M., Seegmiller, H. L., and Marvin, J. G., "Time-Dependent Behavior of a Reattaching Shear Layer," *AIAA Journal*, Vol. 25, No. 7, 1987, pp. 914–919.

[6]Thomas, A. S. W., "The Unsteady Characteristics of Laminar Juncture Flow," *Physics of Fluids*, Vol. 30, No. 2, 1987, pp. 283–285.

[7]Visbal, M. R., "Structure of Laminar Juncture Flows," *AIAA Journal*, Vol. 29, No. 8, 1991, pp. 1273–1282.

[8]Bogar, T. J., "Structure of Self-Excited Oscillations in Transonic Diffuser Flows," *AIAA Journal*, Vol. 24, No. 1, 1986, pp. 54–61.

[9]Erengil, M. E. and Dolling, D. S., "Physical Causes of Separation Shock Unsteadiness in Shock Wave / Turbulent Boundary Layer Interactions," AIAA Paper 93-3134, July 1993.

[10]Brusniak, L. and Dolling, D. S., "Physics of Unsteady Blunt-Fin-Induced Shock Wave / Turbulent Boundary Layer Interactions," *Journal of Fluid Mechanics*, Vol. 273, 1994, pp. 375–409.

[11]Smith, M. W., *Flow Visualization in Supersonic Turbulent Boundary Layers*, Ph.D. thesis, Princeton University, Princeton, NJ, 1989.

[12]Smith, D. R., Poggie, J., Konrad, W., and Smits, A. J., "Visualization of the Structure of Shock Wave Turbulent Boundary Layer Interactions using Rayleigh Scattering," AIAA Paper 91-0651, January 1991.

[13]Forkey, J., Cogne, S., Smits, A., and Bogdonoff, S., "Time-Sequenced and Spectrally-Filtered Imaging of Shock Wave and Boundary Layer Structure for Inlet Characterization," AIAA Paper 93-2300, June 1993.

[14]Lempert, W. R., Wu, P.-F., and Miles, R. B., "Filtered Rayleigh Scattering Measurements using a MHz Rate Pulse-Burst Laser System," AIAA Paper 97-0500, January 1997.

[15]Kussoy, M. I., Brown, J. D., Brown, J. L., Lockman, W. K., and Horstman, C. C., "Fluctuations and Massive Separation in Three-Dimensional Shock-Wave / Boundary-Layer Interactions," *Transport Phenomena in Turbulent Flows: Theory, Experiment, and Numerical Simulation*, Hemisphere, New York, 1988, pp. 875–887.

[16]Dolling, D. S. and Murphy, M. T., "Unsteadiness of the Separation Shock Wave Structure in a Supersonic Compression Ramp Flowfield," *AIAA Journal*, Vol. 21, No. 12, 1983, pp. 1628–1634.

[17]Hayashi, M., Aso, S., and Tan, A., "Fluctuation of Heat Transfer in Shock Wave / Turbulent Boundary Layer Interaction," *AIAA Journal*, Vol. 27, No. 4, 1989, pp. 399–404.

[18]Shifen, W. and Qingquan, L., "Hypersonic Turbulent Separated Flow Past an Unswept Circular Cylinder on a Flat Plate," *Acta Aerodynamica Sinica*, Vol. 10, No. 1, 1992, pp. 38–44.

[19]Erengil, M. E. and Dolling, D. S., "Correlation of Separation Shock Motion with Pressure Fluctuations in the Incoming Boundary Layer," *AIAA Journal*, Vol. 29, No. 11, 1991, pp. 1868–1877.

[20]Shen, Z.-H., Smith, D. R., and Smits, A. J., "Wall Pressure Fluctuations in the Reattachment Region of a Supersonic Free Shear Layer," *Experiments in Fluids*, Vol. 14, No. 1/2, 1993, pp. 10–16.

[21]Plotkin, K. J., "Shock Wave Oscillation Driven by Turbulent Boundary-Layer Fluctuations," *AIAA Journal*, Vol. 13, No. 8, 1975, pp. 1036–1040.

[22]Brusniak, L. and Dolling, D. S., "Engineering Estimation of Fluctuating Loads in Shock Wave / Turbulent Boundary-Layer Interactions," *AIAA Journal*, Vol. 34, No. 12, 1996, pp. 2554–2561.

[23]Erlebacher, G. and Hussaini, M. Y., "On Shock Shape Alteration Due to Interaction with Organized Structures," AIAA Paper 99-3526, June/July 1999.

[24]Baca, B. K., *An Experimental Study of the Reattachment of a Free Shear Layer in Compressible Turbulent Flow*, Master's thesis, Princeton University, Princeton, NJ, 1981.

[25]Horstman, C. C., Settles, G. S., Williams, D. R., and Bogdonoff, S. M., "A Reattaching Free Shear Layer in Compressible Turbulent Flow," *AIAA Journal*, Vol. 20, No. 1, 1982, pp. 79–85.

[26]Settles, G. S., Williams, D. R., Baca, B. K., and Bogdonoff, S. M., "Reattachment of a Compressible Turbulent Free Shear Layer," *AIAA Journal*, Vol. 20, No. 1, 1982, pp. 60–67.

[27]Hayakawa, K., Smits, A. J., and Bogdonoff, S. M., "Turbulence Measurements in a Compressible Reattaching Shear Layer," *AIAA Journal*, Vol. 22, No. 7, 1984, pp. 889–895.

[28]Samimy, M., Petrie, H. L., and Addy, A. L., "A Study of Compressible Turbulent Reattaching Free Shear Layers," *AIAA Journal*, Vol. 24, No. 2, 1986, pp. 261–267.

[29]Samimy, M. and Addy, A. L., "Interaction Between Two Compressible, Turbulent Free Shear Layers," *AIAA Journal*, Vol. 24, No. 12, 1986, pp. 1918–1923.

[30]Smith, K. M. and Dutton, J. C., "Investigation of Large-Scale Structures in Supersonic Planar Base Flows," *AIAA Journal*, Vol. 34, No. 6, 1996, pp. 1146–1152.

[31]Papamoschou, D. and Roshko, A., "The Compressible Turbulent Shear Layer: An Experimental Study," *Journal of Fluid Mechanics*, Vol. 197, 1988, pp. 453–477.

[32]Poggie, J., *On the Control of a Compressible, Reattaching Shear Layer*, Ph.D. thesis, Princeton University, Princeton, NJ, 1995.

[33]Cogne, S., Forkey, J., Lempert, W., Miles, R. B., and Smits, A. J., "Evolution of Large-Scale Structures in a Supersonic Turbulent Boundary Layer," *Transitional and Turbulent Compressible Flows,* ASME FED-vol. 151, The American Society of Mechanical Engineers, New York, 1993, pp. 229–237.

[34]Wegener, P. P. and Pouring, A. A., "Experiments on Condensation of Water Vapor by Homogeneous Nucleation in Nozzles," *The Physics of Fluids*, Vol. 7, No. 3, 1964, pp. 352–361.

[35]Shirinzadeh, B., Hillard, M. E., and Exton, R. J., "Condensation Effects on Rayleigh Scattering Measurements in a Supersonic Wind Tunnel," *AIAA Journal*, Vol. 29, No. 2, 1991, pp. 242–246.

[36]Nau, T., *Rayleigh Scattering as a Quantitative Tool in Compressible Turbulent Boundary Layers*, Master's thesis, Princeton University, Princeton, NJ, 1995.

[37]Poggie, J., "Quantitative Visualization of Supersonic Flow Using Rayleigh Scattering," AIAA Paper 96-0436, January 1996.